RSC Advances

ROYAL SOCIETY OF CHEMISTRY

www.rsc.org/advances

Novel hybrid photocatalytic reactor-UF nanocomposite membrane system for bilge water degradation and separation

A. Moslehyani[a,b], A. F. Ismail[a,b,*], M. H. D. Othman[a,b], Arun M. Isloor[c]

[a] *Advanced Membrane Technology Research Centre (AMTEC), Universiti Teknologi Malaysia, 81310 UTM Skudai, Johor Darul Ta'zim, Malaysia*

[b] *Faculty of Petroleum & Renewable Energy Engineering, Universiti Teknologi Malaysia, 81310 UTM Skudai, Johor Darul Ta'zim, Malaysia*

[c] *Membrane Technology laboratory , Chemistry Department, National Institute of Technology Karnataka, Surathkal, Mangalore 575 025, India*

*Corresponding author: afauzi@utm.my; fauzi.ismail@gmail.com, Tel: +607-5535592, Fax: +607-55355925

Graphical abstract

Bilge water degradation and separation via hybrid photocatalytic membrane reactor based on polyvinylidene fluoride (PVDF)/halloysite nanotube clay (HNTs) nanocomposite membrane has been achieved by this study.

Abstract

This study focuses on the design and performance of a hybrid system consisting of a photocatalytic reactor and ultrafiltration permeation cell. Initially, an ultraviolet (UV) lamp was installed in the photocatalytic reactor to decompose the bilge organic pollutants in the presence of 200 ppm titanium-dioxide (TiO_2). Individual hydrocarbon compounds of bilge water samples were identified by gas chromatography-mass spectrometry (GC-MS) analysis. Two types of membrane, which are pure polyvinylidene fluoride (PVDF) membrane and PVDF/modified halloysite nanotube clay (M-HNTs) nanocomposite membrane was fabricated aiming to enhance the rejection, flux and fouling resistance for full filtration of pollutants from photocatalytic reactor. Membranes were characterized by Fourier transform infrared (FTIR), field emission scanning electron microscopy (FESEM) and atomic force microscopy (AFM). Furthermore, GC-MS analysis showed that, over 90% bilge

decomposition occurred by photocatalytic reaction. The TiO_2 cross-over during permeation was detected by using atomic absorption spectrophotometer (AAS), which proved that, TiO_2 rejection was more than 99% for nanocomposite membrane. UV−vis spectrophotometer confirmed over 99% rejection of decomposed bilge hydrocarbon via nanocomposite membrane with 1.0 wt.% of M-HNTs incorporated in PVDF matrix.

Keywords: Photocatalytic reactor, UF, nanocomposite membrane, PVDF, HNTs, bilge water

1. Introduction

Bilge water is a kind of toxic and corrosive oily wastewater in the ships [1], as it illustrated in Fig. 1. This oily wastewater is commonly discharged to the marine environment without an appropriate treatment [2], which contributing to a major pollution in the marine ecosystems and affecting marine life [3]. International Maritime Organization (IMO) has set the maximum oil content for the ship discharge should not be more than 15 ppm according to MARPOL 73/78 Convention [4]. On the other hand, according to Malaysia Sewage and Industrial Effluent Discharge Standards regulation and European Union (EU), the grease and oil concentration in discharge water should not be more than 10 ppm and 5 ppm, respectively [5, 6]. Meaningful, a high performance on-board bilge water purifier is necessary for all ships [7]. Currently, the focus of the ship industries is more on the bilge water degradation and separation via developed and low-cost technologies [7, 8]. In particular, bilge water from the ships which includes various hydrocarbons such as alkanes, alkenes, alkynes, cycloalkanes and arenes necessitates efficient demulsification technique [9]. Lately, the combination of photooxidation and membrane separation has attracted the interest of researchers to degrade and purify bilge organic compounds [10, 11].

In particular, photooxidation by photocatalytic reactor is known as one of the novel techniques of advanced oxidation processes (AOPs) [12, 13]. It has been used to decompose the organic and inorganic compounds [10, 11]. Photooxidation parameters of photocatalytic reactors are playing an important role for this hybrid process [14]. One of the most important parameter is photocatalyst type and loading [15], which can affect the performance of the process [10, 11]. Titanium dioxide (TiO_2) as a best photocatalyst to the present work has been well-accepted due to its high photooxidation performance and recovery capability[16]. Furthermore, TiO_2 has

also high reactivity with ultraviolet (UV) light due to electrons promoted by the valance band and conduction band of the semi-conducting oxide for electron–hole pairs[17].

Fig. 1.

On the other hand, presence of decomposed pollutant by photocatalyst in the photocatalytic reactor combines it to proper filtration system[18, 19]. Hence, ultrafiltration (UF) membrane as a suitable filtration processes [19-21] has that capability to be combined with photocatalytic reactor [22] to separate decomposed material and photocatalyst from the photocatalytic reactor [10, 23]. Low cost property and high efficient separation are the UF beneficial in this approach [24, 25], which is already experimented for the TiO_2 and hydrocarbon filtration separately [25-27]. Combination of photocatalytic reactor and UF process is expected to be as an effective hybrid system for the full treatment of bilge water. However, the bilge retentate adsorption and TiO_2 cake layer on the UF membrane surface or in the UF membrane pores causes membrane fouling [28]. Thus, high performance UF membrane production is an another challenging area for any process [29-31].

UF nanocomposite membranes as an alternative solution have shown a promising property for water purification technologies [32]. UF nanocomposite membrane has been usually fabricated using organic and inorganic nanofillers [33], which requires well dispersion inside the polymer matrix to achieve a high-performance nanocomposite membrane [34]. On the other hand, nanofiller selection in terms of mechanical and economical beneficial property is another significant factor [35]. Halloysite nanotubes (HNTs) as one of the promising nanofillers is a type of aluminosilicate clay [36] with the high chemical and physical property [37] for superior applications in multiple field due to its morphological structure [38]. Some of the HNTs properties are as follow; flux developer, anti-fouler, low cost material [39]. However, major drawback of these nanofiller is its agglomeration, which need to be reduced by chemical modification of HNTs using silane or suitable acid [40].

Therefore, high efficient hybrid design and promising UF nanocomposite membrane for bilge water photooxidation and separation is the main objective of this investigation. In particular, polyvinylidene fluoride (PVDF) was chosen to be the base polymeric membrane due to its superior mechanical and membrane forming characteristics and modified HNTs (M-HNTs) was selected as membrane nanofiller.

2. Experimental

2.1. Materials

Nanocomposite membranes materials of this report are as follow; polymer was polyvinylidene fluoride (PVDF) Solef 6012 purchased from Solvay Advanced Polymers, solvent was dimethylacetamide (DMAc, >99.5%) from Merck, nanocomposite filler was halloysite nanotubes (HNTs) clay with inner tube diameter of 5-15 nm from Sigma Aldrich, nanocomposite filler modifier was N-β-(aminoethyl)-ɣ-aminopropyltrimethoxy silane (AEAPTMS) from Merck. Toluene and tetra hydro furane (THF) from QReC were used for HNTs modification and modified HNTs washing respectively. On the other hand, photocatalyst of the study was titanium-dioxide (TiO_2) P25 nanoparticles from Evonik Degussa with BET surface area of 50±15 m^2/g.

2.2. HNTs modification technique

HNTs was modified by following procedure; firstly, HNT was kept inside oven to remove moisture at 70 ^oC for 72 h then AEAPTMS and HNTs (1:2) (wt/wt) % dissolved in 400 ml toluene for 6 h sonication at 65 ^oC. After that, reaction mixture was agitated by using magnetic stirrer at 65 ^oC for one night while agitation was ended the modified HNTs (M-HNTs) was washed with 400 ml of THF, and followed by 400 ml of de-ionized water by centrifuging to remove non reacted AEAPTMS from modified HNTs surface. After that, M-HNTs was kept in oven at 95 ^oC for another 48 h. Dried M-HNTs powder has been ball milled using mixer to avoid any adhesion among M-HNTs [41, 42].

2.3 Nanocomposite membrane formulation and fabrication

Fabricated membranes were denoted as follow; PVDF/DMAc (M1), and PVDF/DMAc/M-HNTs (M2), and their composition is listed in Table 1 in detail. In order to achieve best nanoparticles dispersions in the dope, agitation was performed within the speed of 350 rpm and temperature of 65 ^oC for at least one day. The polymeric solution was casted uniformly on a glass substrate with the thickness of 250 μm. After that casted flat sheet membrane was immersed into the distilled water (for 3 days) and mixture of methanol distilled water 2:1 (v/v) % bath (for 5 hr), respectively [43, 44].

Table 1

Casting solution compositions

Membrane	Membrane code	(w/w) %		
		NT	PVDF	DMAc
Pure PVDF	M1	0.0	18.0	82.0
M-HNT/PVDF	M2	1.0	18.0	81.0

2.4 Characterization of the prepared membrane

An ATR-IR spectrum of nanocomposite membrane was recorded using Perkin Elmer 1650 to confirm the presence of M-HNTs in the membrane matrix. Typically, 84 scans were signal-averaged to reduce spectral noise. Thermal gravimetric analysis (TGA) of nanocomposite membranes was archived using a TG-DTA, DT-40 system (Shimadzu, Japan), in which 3 mg of each membrane sample was heated (from 0 to 800 ^{o}C at the rate 10 ^{o}C/min) under nitrogen flow [45]. Cross-sectional structure of nanocomposite membrane was observed using field emission scanning electron microscope (FESEM, Jeol JSM 6701-F) combined with energy dispersive X-ray (EDX- Jeol JED-2300F). Hydrophilicity of the nanocomposite membrane was achieved via water contact angle analyzer (model IMC-159D by IMOTO Machinery Co. Ltd.) by dropping of 5 µl de-ionized water to the membrane surface. On the other hand, atomic force microscopy (AFM) was done for knowing the roughness of the prepared membrane. The membrane surfaces was imaged in a scan size of 5µm×5µm. The average roughness (S_a), the root mean square of Z data (S_q) the mean difference between the highest peaks and lowest valleys (S_z) and the root mean square [46]. The mean pore size, μ_p (nm), was also determined from the AFM image of the membrane surface by the method developed by Singh *et al*, 1998 [47].

2.5 Procedure and analysis

Fig. 2 is illustrating the schematic representation of the hybrid system used in this study, which is combination of a photocatalytic reactor connected to a UF permeation cell. The size

of the photocatalytic reactor is 48 cm x 20 cm x18 cm made of prospect plastic, covered with an aluminum foil to shield ultraviolet type C (UVC) light. The UVC lamp manufactured in UV INDUSTRIES, Johor Bahru, Malaysia with the following properties 185 nm+253.7 nm wavelength, outer diameter 2.2 cm, length 30 cm, power 8 W, which it was placed in the center of the photoreactor. The permeation cell is a batch ultrafiltration cell made from stainless steel. The pressure of the permeation cell was supplied from a nitrogen cylinder. The bilge water was obtained from one of the Eastern Malaysian oil tankers. The physical specifications of bilge water are listed in Table 2.

Table 2

Characterization of bilge wastewater

Parameters	Data
Concentration of hydrocarbons in bilge water at initial time	200 (ppm)
Viscosity of bilge water	1.21 (centipoise)
Initial bilge droplet in photoreactor	0.80 (μm)
Retentate bilge droplet in photoreactor	1.84 (μm)

The bilge water with 200 ppm hydrocarbon concentration has been mixed with TiO_2 photocatalyst with concentration of 200 ppm via 2 h sonication. The photooxidation was achieved by 6 h UVC irradiation. Magnetic stirrer, having 50 rpm was used to reduce the concentration polarization effect in photocatalytic reactor and permeation cell. After 6 h, 200 ml of irradiated bilge water was transferred to the permeation cell and the permeation experiment was started with different operating pressure from 0.5 to 2 bar gauge with 0.5 bar interval. All experiments were conducted at ambient temperature. The samples collected from the photocatalytic reactor before UV irradiation, after 6 h of UV irradiation and after 2 h UF filtration were subjected to GC-MS and to know the effect of hybrid system to decompose and filtrate the bilge water. The concentration of bilge water in PMR and permeate was measured by the UV-VIS spectrophotometer (HACH, DR/5000) at wavelength of 598nm. TiO_2 rejection in the aqueous solution during filtration detected via atomic absorption spectrophotometer (AAS) analysis. This is essentially appropriate to the all permeate samples after each batch of each nanocomposite membrane experiment for all applying pressures.

Fig. 2.

In membrane filtration experiments, permeation flux was measured gravimetrically by Eq. (1) [48]:

$$J = \frac{V}{A \times t} \quad \text{Eq. (1)}$$

where volume of permeate was V (L), membrane effective area was A (m^2), and sampling time was t (h). Bilge rejection percentage R(%) was calculated by Eq (2) [49]:

$$R(\%) = 1 - (\frac{C_P}{C_F}) \times 100 \quad \text{Eq. (2)}$$

where C_P (ppm) is bilge concentration in permeate and C_F (ppm) is the bilge concentration in the PMR, which remained almost the same during the entire PMR operation. Flux decline, FD_t (%) was calculated by Eq. (3) [50]:

$$FD_t(\%) = (1 - \frac{J_{P,t}}{J_{P,i}}) \times 100 \quad \text{Eq. (3)}$$

where $J_{p,t}$ was the flux at time t ($Lm^{-2}h^{-1}$), and $J_{p,i}$ was the initial flux (Lm^{-2} h^{-1}). Flux recovery has been caculated by the Eq. (4) [51]:

$$R_{FR} = \frac{J_{w2}}{J_{w1}} \times 100 \quad \text{Eq. (4)}$$

where J_{w2} was the flux at second time t ($Lm^{-2}h^{-1}$) after membrane back washing, typically t is equal to 1 h, and J_{w1} was the flux at first time (Lm^{-2} h^{-1}), at typically t equal to 1 h.

3. Results and discussion

3.1 Characterization of pure PVDF and nanocomposite membrane

The thermal characteristics of M1 (a) and M2 (b)are illustratedin Fig. 3. The thermal decomposition (T_d) of M2was higher than other membranes, i.e. T_d~ 351.12^{o}C for M1has moved to 483.19^{o}C for M2. This proved that the addition of M-HNTs into the PVDF polymer matrix has increased the thermal stability of M2. Moreover, T_g of PVDF increased by the incorporation of M-HNTs, which is in agreement with the literature [52, 53].

Fig. 3.

Fig. 4 showed ATR-IR spectra of M1 (a) and M2 (b). In all membranes strong absorption band appeared at 1140–1280 cm^{-1} which is the main characteristic of CF_2 functional group of PVDF polymer. Moreover, two peaks at 2893 and 3368 cm^{-1} appeared for M2 which indicates the successful M-HNT incorporation in PVDF matrix [54].

Fig. 4.

The presence of elements in nanocomposite membranes was confirmed by EDX analysis and is listed in Table 3. The surfaces of all membranes have more than 60 wt % of F element which came from PVDF. However, M2 showed relatively lower wt % of F compared to M1. Fig. 5 depicts the FESEM cross-sectional images of M1 (a) and M2 (b), respectively. Accordingly, short finger-like voids of M1 membrane turned into longer and larger finger-like voids of M2. On the other hand, the sponge-like region was shrunk from M1 to M2. Thus, the overall porosity of the membrane increased from M1to M2 due to the M-HNTs and incorporation of the same into the polymer matrix. Together with the ATR-IR observation of membranes, it can be concluded that, modified HNTs were well dispersed and strongly bounded to PVDF matrix.

The hydrophilicity of the membrane surface was further investigated by contact angle and atomic force microscope (AFM, Fig. 6). Mean pore radius size and membrane roughness are summarized in Table 4.Membrane roughness (Sa) was increased from M1 to M2 by incorporation of M-HNTs (refer Fig. 8). This was due to existence of nano fillers in the membrane surface and membrane structure changes with incorporating M-HNTs into the polymer matrix, and make Sz redeemably higher for M2 (see Fig. 11). Moreover, contact angle was decreased by the presence of M-HNTs in M2 due to hydrophilic property of M-HNTs. Thus, the membrane surface became more hydrophilic. The stated results for contact

angle and mean pore size were shown a promising specification for M2, which may affected in the membrane performance.

Table 3

EDX element composition detection

Membrane	Elements (wt%)			
	F	Si	Al	Others
M1	63.45	0.00	0.00	36.55
M2	61.95	0.64	0.12	37.29

Fig. 5.

Fig. 6.

Table 4

Roughness parameters, average pore size and contact angle of the membrane surface

Membrane	Contact angle (^{o})	Mean Pore size (r_m, nm)	AFM roughness parameters		
			S_a (nm)	S_q (nm)	S_z (nm)
M1	78.13±1.35	85.47	4.12±1.6	32.2±2.6	132.8±5.1
M2	47.35±2.36	24.32	15.8±1.3	15.9±1.9	172.4±1.4

3.2 Photocatalytic reactor performance study

Fig. 7 shows the GC-MS chromatograms of the samples collected (a) from the photoreactor before UV irradiation, (b) from the photoreactor after 6 h of irradiation, (c) collected as permeate of the permeation experiment conducted with M1 at 1 bar after operational period, (d) collected as permeate of the permeation experiment conducted with M2 at 1 bar after operational period. According to the GC-MS chromatograms, it can be observed that, many peaks corresponding to hydrocarbons, including aliphatic, alicyclic and aromatic, were observed in the sample (a) collected before irradiation. Many peaks disappeared and the intensities of the remaining peaks have substantially decreased in sample (b) after 6 h of

irradiation due to photooxidation catalyzed by TiO_2 and the total peak area decreased by more than 90% of average from all components due to photocatalytic reactor decomposing process. Practically all peaks have disappeared in the permeate sample (c) and (d). Considering the size of the membrane and those of the hydrocarbon molecules, the removal of the hydrocarbons was achieved by the rejection of large colloidal particles of emulsified hydrocarbons. Interestingly pH dropped from 8.56 of sample (a) to 4.79 of sample (b) indicating the formation of acidic compounds by photooxidation of hydrocarbons, which have not necessarily been detected by GC-MS. The pH returned to 7.21 in sample (c) and 6.89 in sample (d), which indicates the removal of the acidic components by filtration.

Fig. 7.

Generally, GC-MS is not able to detect that, 90 % of hydrocarbon decomposition are equal to 90 % of hydrocarbon rejection. Because, few changes in the compounds was observed by GC-MS, that means known compounds converted in to unknown compounds, which cannot be detected by GC-MS using same column and same method. However, GC-MS and spectrophotometer analysis indicates that overall hydrocarbon decomposition and rejection have been occurred by the hybrid system.

3.3 Membranes performance study

3.3.1 Permeation flux

Fig. 8 shows the flux measured by the permeation experiments in which, the UV irradiated bilge water was filtered by the M1-M2 membranes under different transmembrane pressure drops. The flux decreased with time due to membrane fouling, likely caused by the cake layer formation of TiO_2 particles on the membrane surface or by the adsorption of highly hydrophobic oil layer to the membrane pore wall, blocking the pore partially. Fig. 9 summarizes the flux after 1 h of operation. The figure shows that, the flux kept increasing from M1 to M2. This is due to the increase in hydrophilicity (see contact angle data in Table 4) and the bulk porosity as evidenced by the FESEM cross-sectional images of M1 and M2 membranes (see Fig. 5). Flux changed only marginally, when the transmembrane pressure difference was increased from 0.5 to 2 bar. This is often observed for UF membrane and interpreted by the formation of a cake layer deposited on the surface of the membrane. In this

study the thickness of the deposited TiO_2 layer has increased progressively with an increase in transmembrane pressure difference, offsetting the increase in the driving force.

Fig. 8.

Fig. 9.

3.3.2 Rejection

Fig. 10 shows the percent rejection of the irradiated bilge hydrocarbon, by the fabricated membranes at different pressures. It should be noted that, the data are based on the permeate sample collected after 1 h of operation. The figure shows that the rejection was more than 95.5% at the transmembrane pressure difference of 1 bar. Moreover, the rejection was increased to 99.7 % in M2 most likely due to the decrease in the pore size at the membrane surface (see Table 4). Together with the highest flux, M2 membrane was the more favorable among two fabricated membranes. On the other hand, M1 membrane with zero filler loading is the least favorable, which is in good agreement with the earlier work [6]. However, the rejection decreased with the increase in the pressure because the oily components adsorbed at the pore wall, which forced to pass through the pores. It is also worth to note that, European Union (EU) has set a standard for the oil and grease discharge, which should not be more than 5 ppm [6]. Thus, all membranes that were fabricated in this work have met the requirement at the operating pressure of 1 bar gauge.

Fig. 10.

Moreover, Table 5 shows Levels of total organic carbon (TOC) was monitored for both applied membrane to show the effectiveness of photooxidation and membrane separation in this study. The TOC value determined for the all feed at 598.23 ppm, which was reduced ~ 67% after irradiation. Finally after separation process the permeate water TOC was shown ~ 12 ppm for M1 and ~13 ppm for M2 as well. On the other hand, Table 5 shows TiO_2 rejection by the prepared membrane after 1 h filtration test. Obviously, TiO_2 suspended particles in the bilge water were filtered almost completely by M2 membrane. The main concept that may improve the TiO_2 rejection is the membrane pore size. Particularly, suspended TiO_2 in retentae can be recovered via retentate dilution using water and heat up to 250 ^oC for 5 [56] after membrane separation.

Table 5

TiO_2 loss and TOC result at 1 h and 0.5 bar prresure guage

Membrane	TiO_2 rejection (%)[a]	Levels of total organic carbon (TOC) (ppm)			
		Feed	After irradiation	Permeate	Retentate
M1	42.7 ±2.4	598.23±1.2	195.49±3.6	12.49±2.9	81.27±2.3
M2	99.1± 3.7	598.23±1.2	195.53±5.8	13.35±1.1	82.51±1.7

3.3.3 Fouling and anti-fouling property of membranes

Fig. 11a summarizes the flux decline (FD) calculated by Eq. (3) corresponding to t = 1 h, at different pressures for all the fabricated membranes. In the figure, FD of the M2 is lower than M1 and the trends decreased with the operating pressure. There are three resistance for the transport of permeate through the membrane such as, a) resistance of the membrane, b) resistance of the cake layer formed on the top of the membrane and c) resistance due to the partial blocking of the pore [49].

Fig. 11.

Among those a) is permanent and does not change with time. The resistances b) and c) are enlarging with time and flux declines due to the fouling. Between b) and c), if b) is dominant FD of M2 is supposed to be the highest due to the most severe concentration polarization because both solute rejection and flux of M2 are higher than M1. However, the experimental results presented in Fig. 11 were not in agreement with the expected results. On the other hand, the shear force working on the oily layer adsorbed at the membrane pore becomes stronger as the pore size decreases [57], which makes the adsorbed layer more mobile, resulting in decrease in FD. This is further supported by the decrease of FD with increasing operating pressure, which also increases the shear force at the pore wall [57]. On the other hand, Fig. 11b was showed %FR of pure PVDF and nanocomposite membrane at 1 h of operation for all transmembrane pressures, which was calculated by using Eq. (4). Accordingly, M2 found to be anti-foulant membrane, as compared to the M1. M-HNT and effective back wash solution (hydrochloric acid and water by 1:10 (v/v) %) was the main cause of this behavior. Moreover, after first backwash the membrane flux shown approximately same result,

however after second backwash membrane flux has decreased overall more than ~25 % and after third time backwash the membrane was unusable.

4.0 Conclusions

A novel hybrid system was studied for the removal of bilge water treatment. TiO_2 photocatalyst was suspended in photoreactor for bilge degradation and nanocomposite membrane was fully filtrating via ultrafiltration cell. From the experimental results, the following conclusions can be drawn.

1. A novel designed hybrid system has been shown a great result in terms of fully bilge degradation and separation with the almost green remained waste.
2. More than 90 % of the hydrocarbons were removed in the photoreactor by 6 h photoby UVC irradiation in the presence of TiO_2 photocatalyst.
3. More than 99 % of bilge hydrocarbon and TiO_2 photocatalyst was also removed by filtration by using nanocomposite membrane that contains 1 wt.% of M-HNTs. Hence, the water product was almost free from any organic and inorganic contaminants.
4. Nanocomposite membrane has shown promising result in terms of a parameter permeate flux, fouling and antifouling, matrix compare to pure PVDF membrane due to the excellent nanofiller selection and modification.

Acknowledgement

The authors gratefully acknowledge financial support from the European Commission FP7 - LIMPID (Project number: NMP3-SL-2012-310177, UTM reference: R.J130000.7609.4C031) and technical support from both Aquakimia Sdn. Bhd. and Research Managem ent Centre, Universiti Teknologi Malaysia. The authors also acknowledge Solvay Specialty Polymers Italy and Johnson Matthey PLC UK for providing materials used in this work. AMI thank, Director, NITK Surathkal, India for providing the research facilities.

References

1. M. Asselin, P. Drogui, S. K. Brar, H. Benmoussa and J.-F. Blais, *Journal of hazardous materials*, 2008, **151**, 446-455.

2. C. Copeland, Cruise ship pollution: Background, laws and regulations, and key issues, 2007.
3. J. R. Portela, J. Sanchez-Oneto, J. López, E. Nebot and E. Martinez de la Ossa, *Engineering in life sciences*, 2003, **3**, 85-89.
4. M. M. D. Neves, 2010.
5. H. A. Aziz, M. N. Adlan and K. S. Ariffin, *Bioresource Technology*, 2008, **99**, 1578-1583.
6. B. Chakrabarty, A. Ghoshal and M. Purkait, *Journal of Membrane Science*, 2008, **325**, 427-437.
7. P. Hearn, Google Patents, 1999.
8. C. Sun, T. Leiknes, J. Weitzenböck and B. Thorstensen, *Desalination*, 2009, **236**, 56-64.
9. N. Olivera, M. Commendatore, A. Moran and J. Esteves, *Journal of Industrial Microbiology and Biotechnology*, 2000, **25**, 70-73.
10. M. Padaki, R. S. Murali, M. Abdullah, N. Misdan, A. Moslehyani, M. Kassim, N. Hilal and A. Ismail, *Desalination*, 2015, **357**, 197-207.
11. M. N. Chong, B. Jin, C. W. Chow and C. Saint, *Water research*, 2010, **44**, 2997-3027.
12. A. Moslehyani, A. Ismail, M. Othman and T. Matsuura, *RSC Advances*, 2015.
13. A. Heller, *Accounts of Chemical Research*, 1995, **28**, 503-508.
14. R. Andreozzi, V. Caprio, A. Insola and R. Marotta, *Catalysis today*, 1999, **53**, 51-59.
15. J. J. Pignatello, E. Oliveros and A. MacKay, *Critical reviews in environmental science and technology*, 2006, **36**, 1-84.
16. A. Fujishima, T. N. Rao and D. A. Tryk, *Journal of Photochemistry and Photobiology C: Photochemistry Reviews*, 2000, **1**, 1-21.
17. M. Ni, M. K. Leung, D. Y. Leung and K. Sumathy, *Renewable and Sustainable Energy Reviews*, 2007, **11**, 401-425.
18. X. Huang, M. Leal and Q. Li, *Water research*, 2008, **42**, 1142-1150.
19. B. Van den Bogaert, D. Havaux, K. Binnemans and T. Van Gerven, *Green Chemistry*, 2015.
20. M. A. Masuelli, *Nature*, 2013, **1**, 37-44.
21. A. Lambert, P. Plucinski and I. V. Kozhevnikov, *Chemical Communications*, 2003, 714-715.
22. G. Puma, *Chemical Communications*, 2007, 4749-4751.
23. M. R. Hoffmann, S. T. Martin, W. Choi and D. W. Bahnemann, *Chemical reviews*, 1995, **95**, 69-96.
24. O. Lorain, B. Hersant, F. Persin, A. Grasmick, N. Brunard and J. M. Espenan, *Desalination*, 2007, **203**, 277-285.
25. R. Stoenescu and W. Meier, *Chemical Communications*, 2002, 3016-3017.
26. S.-A. Lee, K.-H. Choo, C.-H. Lee, H.-I. Lee, T. Hyeon, W. Choi and H.-H. Kwon, *Industrial & engineering chemistry research*, 2001, **40**, 1712-1719.
27. X. Zhang, T. Zhang, J. Ng and D. D. Sun, *Advanced Functional Materials*, 2009, **19**, 3731-3736.
28. M. Tomaszewska, A. Orecki and K. Karakulski, *Desalination*, 2005, **185**, 203-212.
29. B.-H. Jeong, E. Hoek, Y. Yan, A. Subramani, X. Huang, G. Hurwitz, A. K. Ghosh and A. Jawor, *Journal of Membrane Science*, 2007, **294**, 1-7.
30. P. G. Jessop, *Green Chemistry*, 2011, **13**, 1391-1398.
31. D. Y. Xing, S. Y. Chan and T.-S. Chung, *Green Chemistry*, 2012, **14**, 1405-1412.
32. J. Huang, K. Zhang, K. Wang, Z. Xie, B. Ladewig and H. Wang, *Journal of membrane science*, 2012, **423**, 362-370.
33. T.-H. Bae, I.-C. Kim and T.-M. Tak, *Journal of Membrane Science*, 2006, **275**, 1-5.

34. L. Yan, S. Hong, M. L. Li and Y. S. Li, *Separation and Purification Technology*, 2009, **66**, 347-352.
35. A. Oya, Y. Kurokawa and H. Yasuda, *Journal of Materials Science*, 2000, **35**, 1045-1050.
36. S. J. Antill, *Australian journal of chemistry*, 2003, **56**, 723-723.
37. S. Hashemifard, A. Ismail and T. Matsuura, *Journal of colloid and interface science*, 2011, **359**, 359-370.
38. A. F. Ismail, S. Hashemifard and T. Matsuura, *Journal of Membrane Science*, 2011, **379**, 378-385.
39. M. Ghanbari, D. Emadzadeh, W. Lau, S. Lai, T. Matsuura and A. Ismail, *Desalination*, 2015, **358**, 33-41.
40. S. Hashemifard, A. Ismail and T. Matsuura, *Chemical Engineering Journal*, 2011, **172**, 581-590.
41. K. Yamada, S. Yoshii, S. Kumagai, I. Fujiwara, K. Nishio, M. Okuda, N. Matsukawa and I. Yamashita, *Japanese journal of applied physics*, 2006, **45**, 4259.
42. Y. Zhang, Y. Chen, H. Zhang, B. Zhang and J. Liu, *Journal of inorganic biochemistry*, 2013, **118**, 59-64.
43. R. Kumar, A. M. Isloor, A. Ismail, S. A. Rashid and T. Matsuura, *RSC Advances*, 2013, **3**, 7855-7861.
44. V. R. Pereira, A. M. Isloor, A. A. Ahmed and A. F. Ismail, *New Journal of Chemistry*, 2015, **39**, 703-712.
45. L.-Y. Yu, Z.-L. Xu, H.-M. Shen and H. Yang, *Journal of Membrane Science*, 2009, **337**, 257-265.
46. K. Khulbe and T. Matsuura, *Polymer*, 2000, **41**, 1917-1935.
47. S. Singh, K. Khulbe, T. Matsuura and P. Ramamurthy, *Journal of Membrane Science*, 1998, **142**, 111-127.
48. S. C. Sutton, M. Rinaldi and K. Vukovinsky, *AAPS PharmSci*, 2001, **3**, 93-97.
49. B. Chakrabarty, A. Ghoshal and M. Purkait, *Chemical Engineering Journal*, 2010, **165**, 447-456.
50. J. Cho, G. Amy and J. Pellegrino, *Journal of Membrane Science*, 2000, **164**, 89-110.
51. R. J. Gohari, E. Halakoo, W. Lau, M. Kassim, T. Matsuura and A. Ismail, *RSC Advances*, 2014, **4**, 17587-17596.
52. R. Wang, G. Jiang, Y. Ding, Y. Wang, X. Sun, X. Wang and W. Chen, *ACS applied materials & interfaces*, 2011, **3**, 4154-4158.
53. L. Y. Yu, H. M. Shen and Z. L. Xu, *Journal of applied polymer science*, 2009, **113**, 1763-1772.
54. G. Socrates, *Infrared and Raman characteristic group frequencies: tables and charts*, John Wiley & Sons, 2004.
55. H. Zhang, X. Lv, Y. Li, Y. Wang and J. Li, *ACS nano*, 2009, **4**, 380-386.
56. S. M. Sajadi, M. Naderi and S. Babadoust, *Journal of Natural Sciences Research*, 2012, **1**, 10-17.
57. O. Le Berre and G. Daufin, *Journal of Membrane Science*, 1996, **117**, 261-270.

Fig.1. Schematic diagram of bilge water sources and bilge water treatment system position in ships

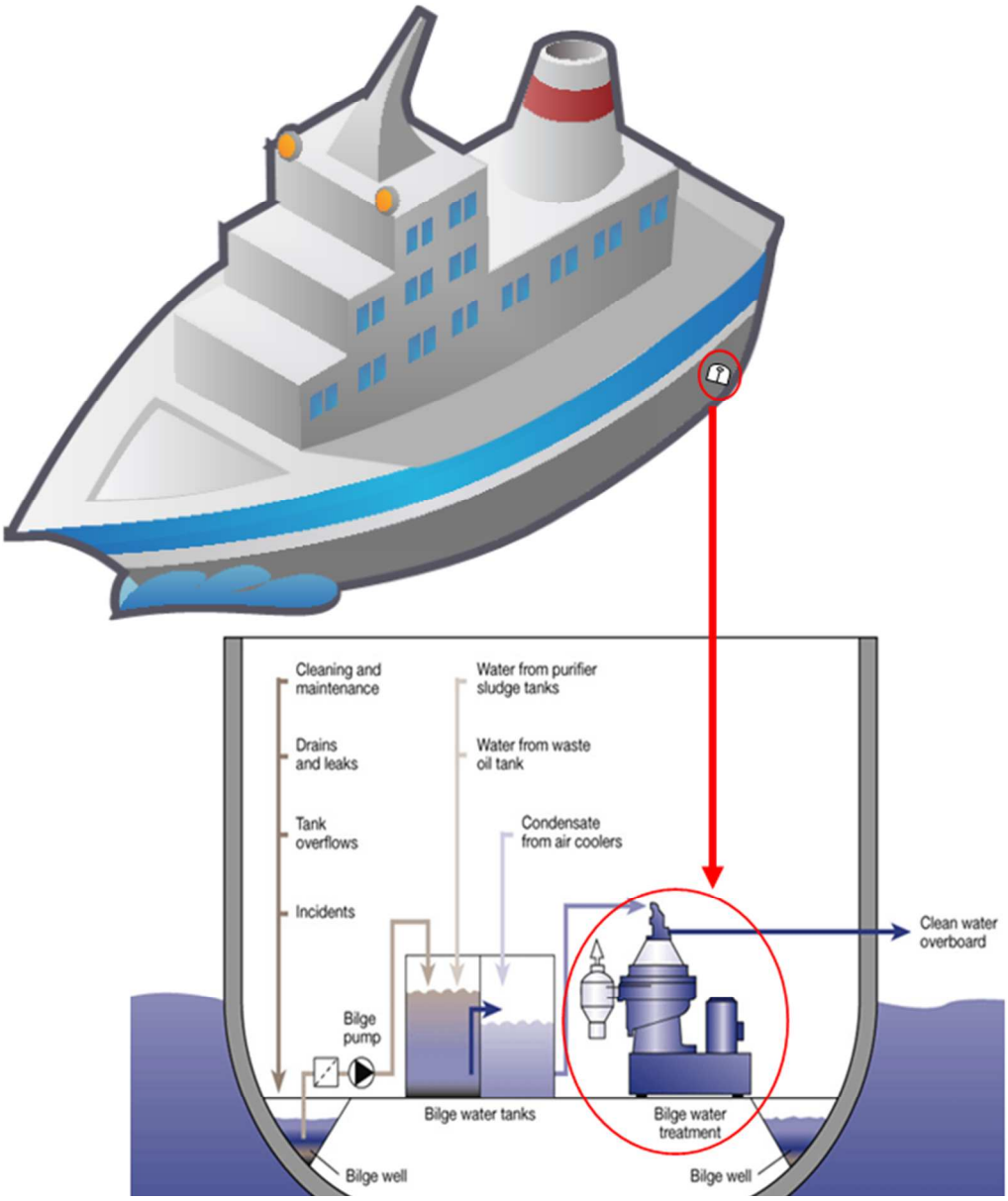

Fig. 2. Schematic diagram of the hybrid system combining photocatalytic reactor and permeation cell

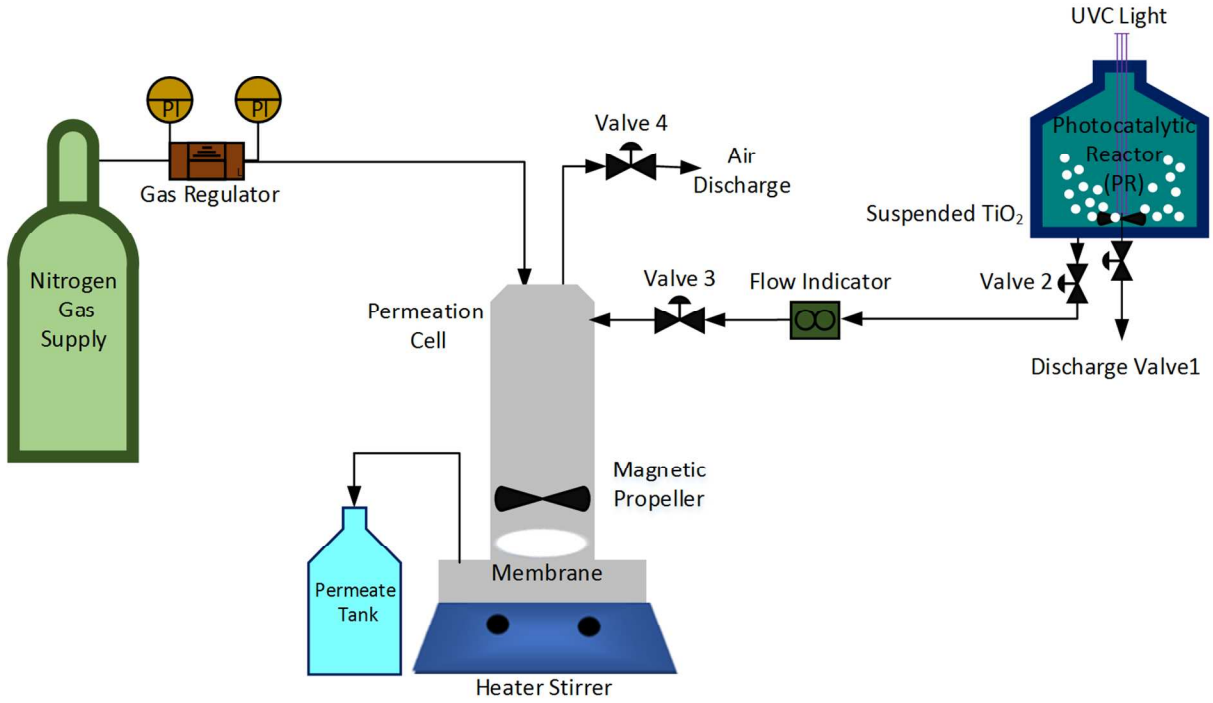

Fig. 3. TGA graph of M1 (a) and M2 (b)

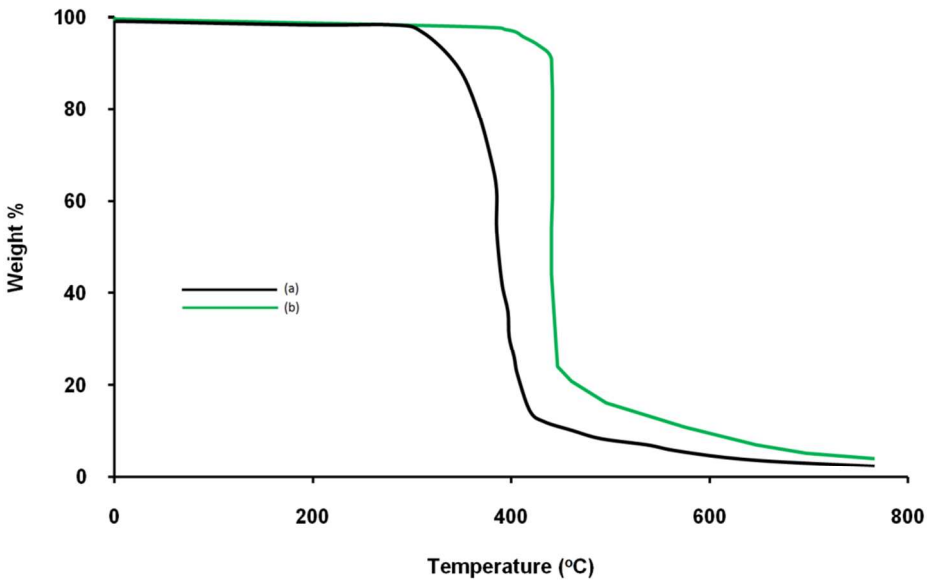

Fig. 4. ATR-IR spectra of M1 (a) and M2 (b)

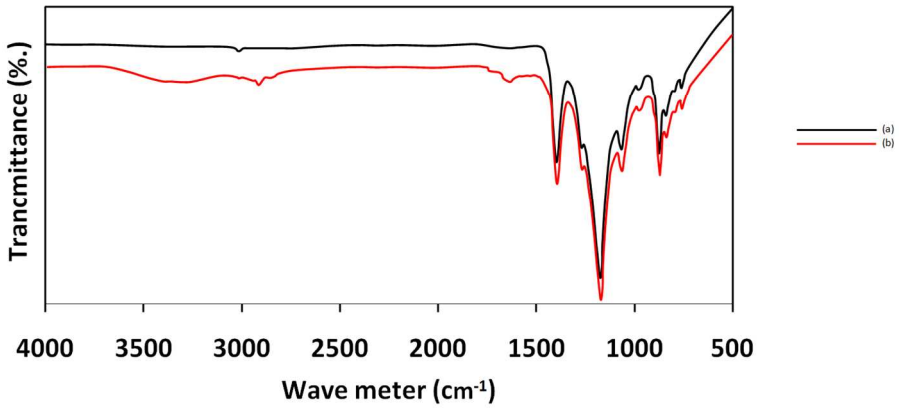

Fig. 5. FESEM cross-sectional images of M1 (a) and M2 (b)

(a)

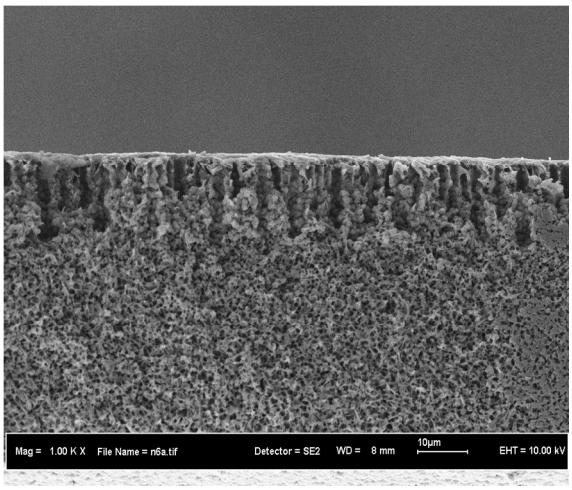

(b)

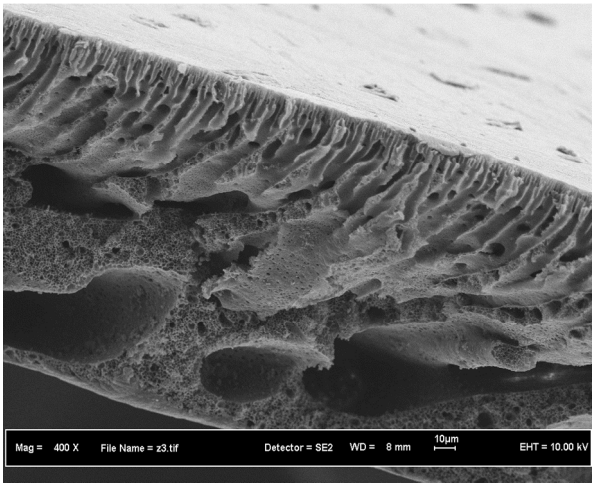

Fig. 6. AFM images of M1 (a) and M2 (b)

M1

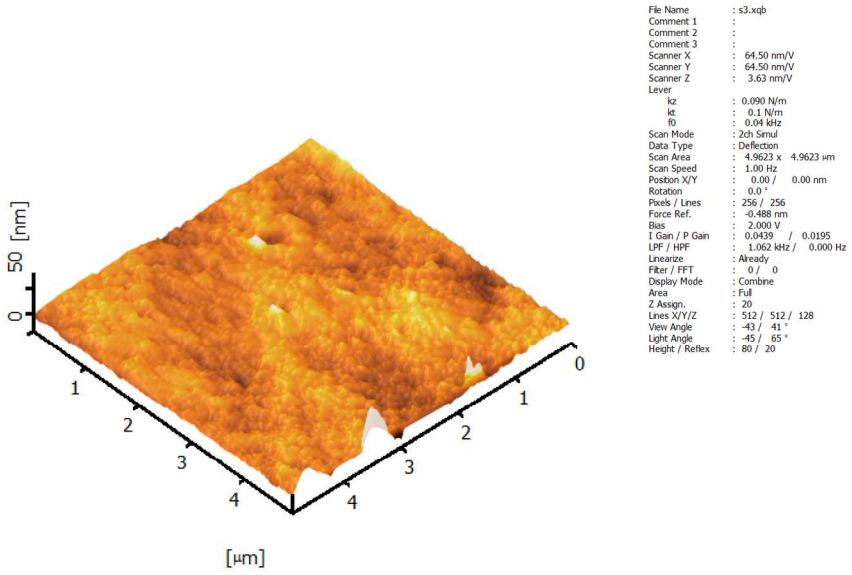

M2

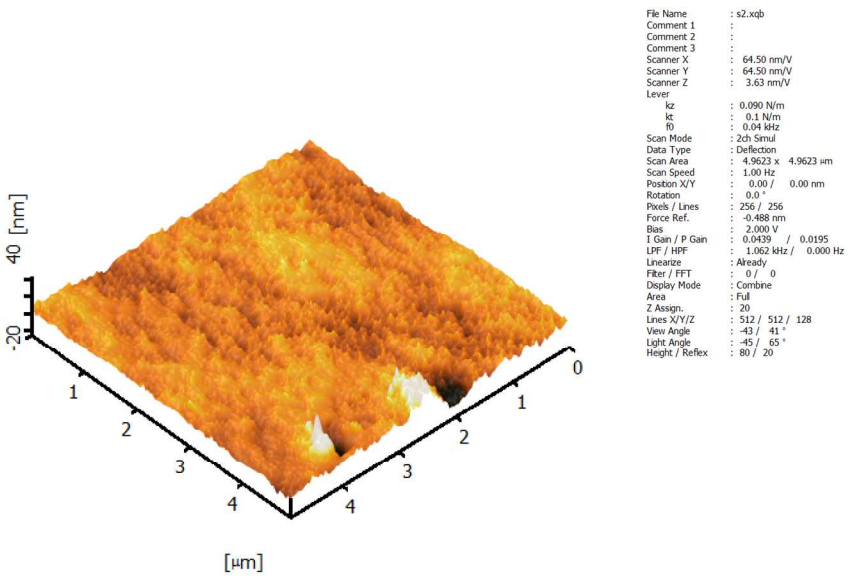

Fig. 7. GCMS chromatograms of a) Original bilge compound quantity b) after 6 h UV irradiation via photocatalytic reactor, c) bilge compound quantity after filtration with M1 at 1 bar after operational period d) bilge compound quantity after filtration with M2 at 1 bar after operational period.

(a)

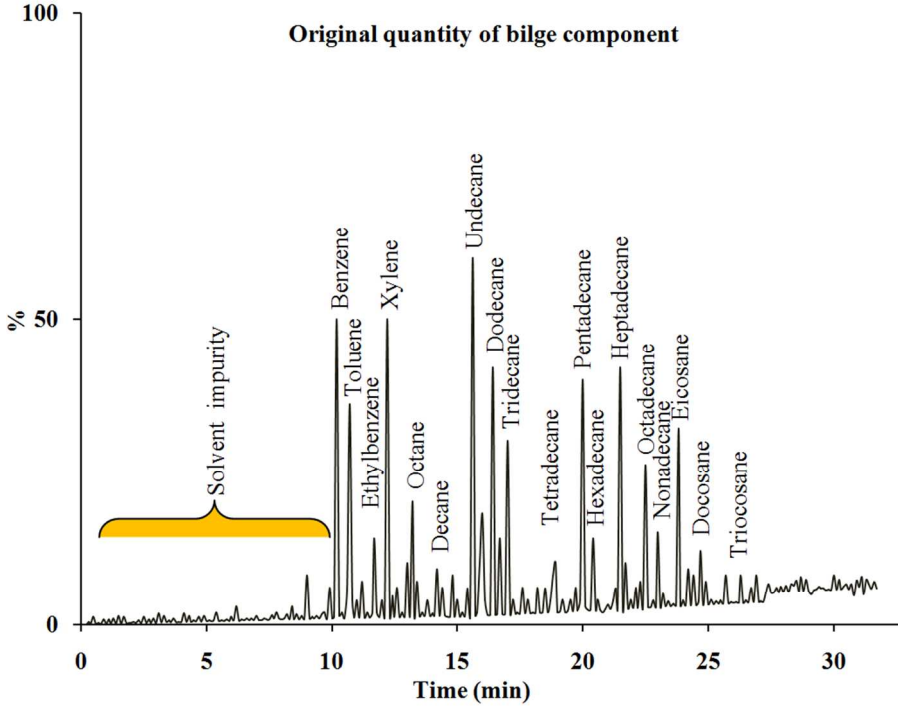

(b)

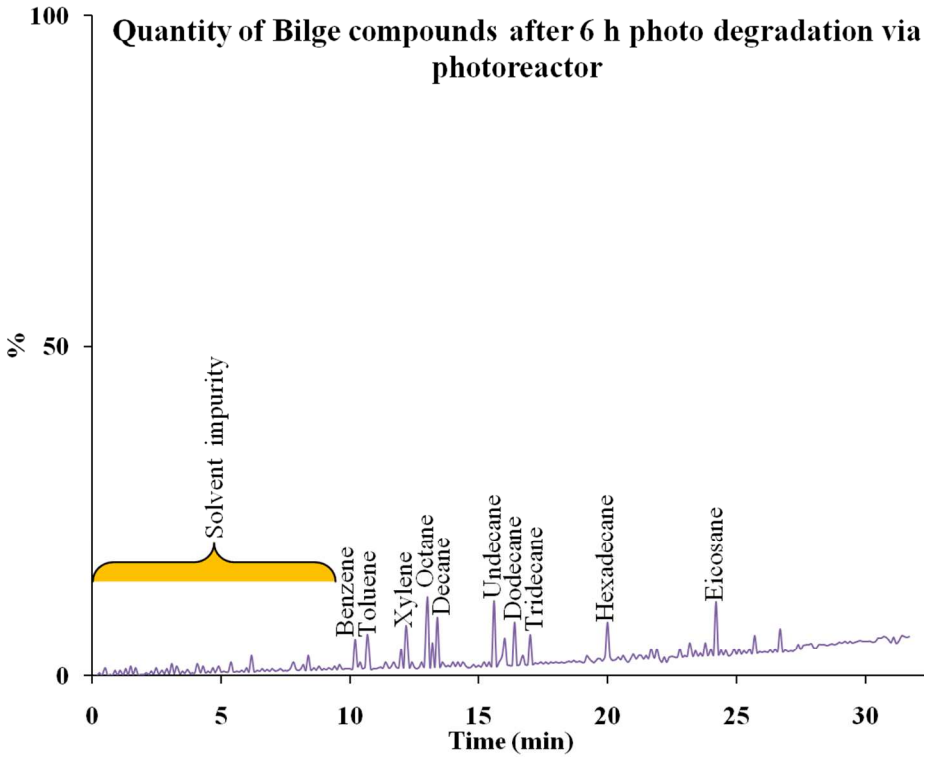

(c)

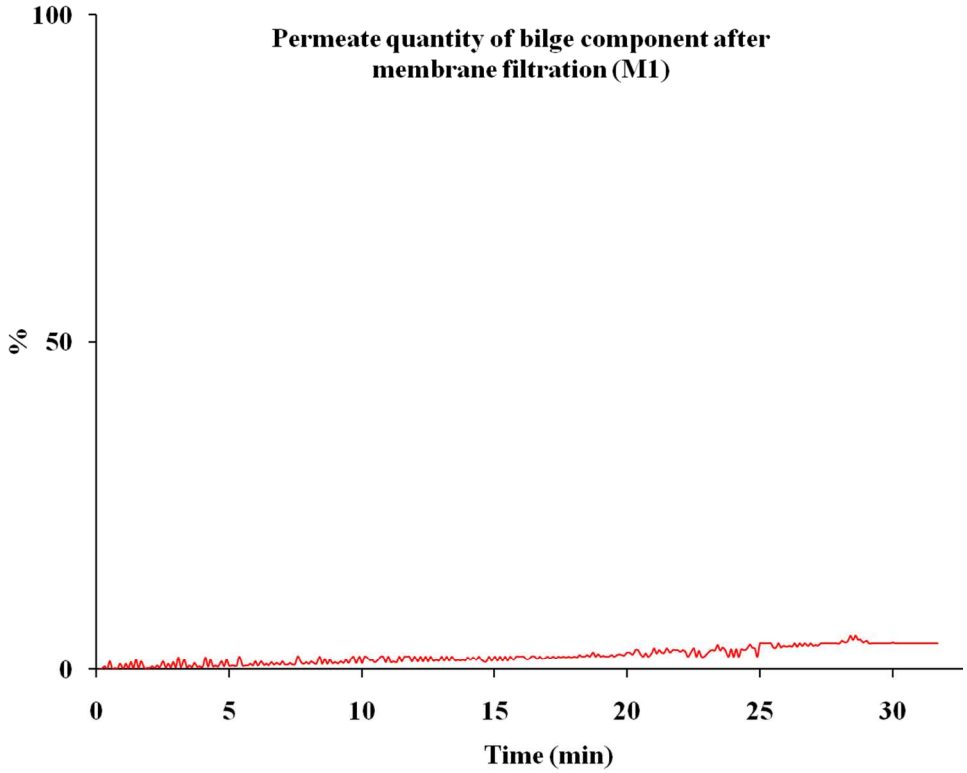

(d)

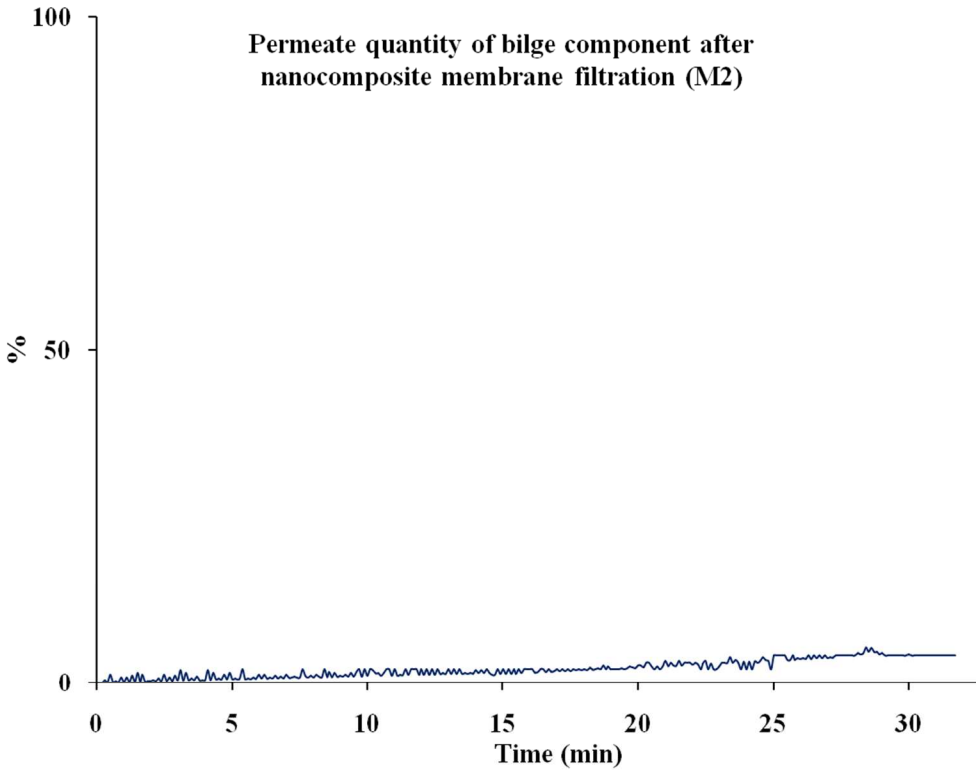

Fig. 8. Permeation flux of M1 (a) and M2 (b)

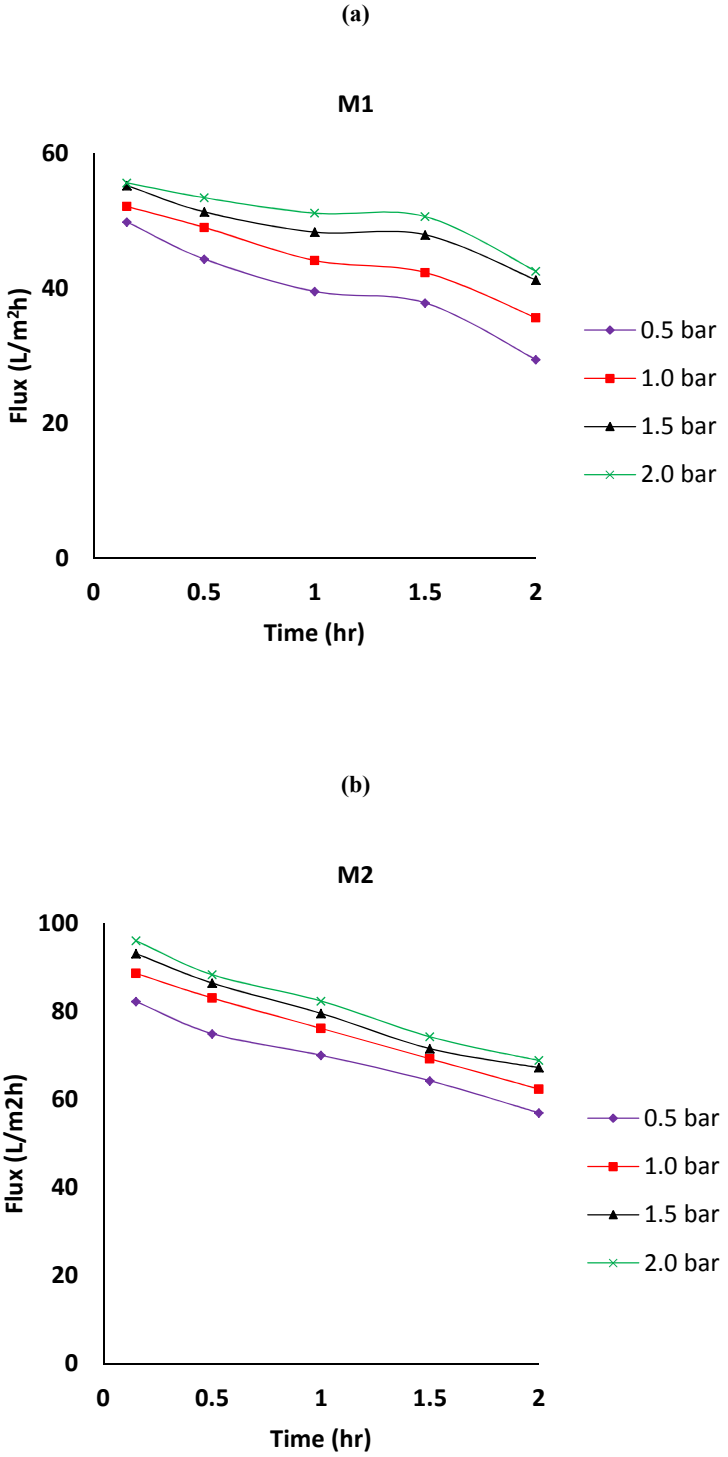

Fig. 9. Effect of transmembrane pressures for M1 and M2 on flux after 1 h filtration

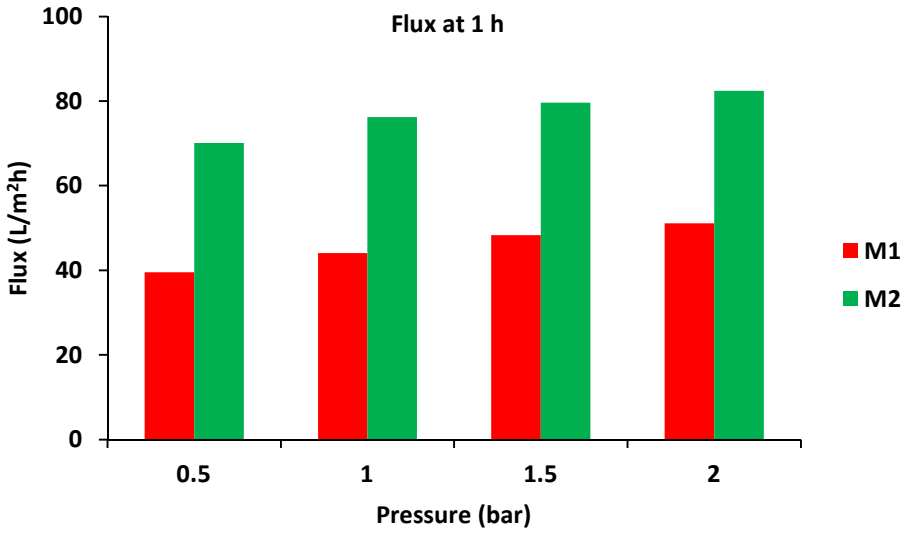

Fig. 10. Rejection of bilge hydrocarbon by the fabricated membranes at different transmembrane pressure difference using hybrid system

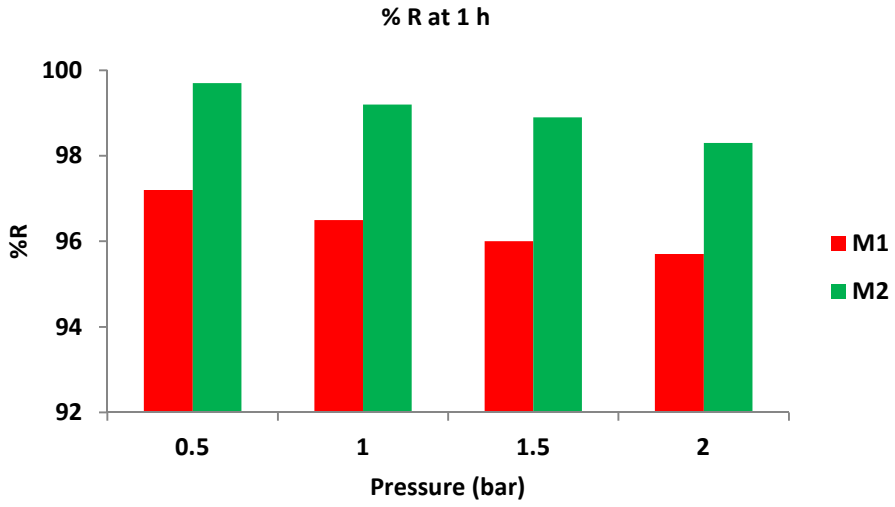

Fig. 11. Flux declination (a) and recovery flux (b) after 1 h of operation at different pressures